SJSU SAN JOSÉ STATE UNIVERSITY

MTI MINETA TRANSPORTATION INSTITUTE

An Ambient NO_X Reduction Reactor System with and without Forced Air

Hamid Rahai, PhD
Komal Gada
Ryan Moffit
Jermey Bonifacio, PhD

CSUTC California State University Transportation Consortium

CALIFORNIA STATE UNIVERSITY LONG BEACH

CSU TRANSPORTATION CONSORTIUM

transweb.sjsu.edu/csutc

MINETA TRANSPORTATION INSTITUTE

Founded in 1991, the Mineta Transportation Institute (MTI), an organized research and training unit in partnership with the Lucas College and Graduate School of Business at San José State University (SJSU), increases mobility for all by improving the safety, efficiency, accessibility, and convenience of our nation's transportation system. Through research, education, workforce development, and technology transfer, we help create a connected world. MTI leads the Mineta Consortium for Emerging, Efficient, and Safe Transportation (MCEEST) funded by the U.S. Department of Transportation, the California State University Transportation Consortium (CSUTC) funded by the State of California through Senate Bill 1 and the Climate Change and Extreme Events Training and Research (CCEETR) Program funded by the Federal Railroad Administration. MTI focuses on three primary responsibilities:

Research

MTI conducts multi-disciplinary research focused on surface transportation that contributes to effective decision making. Research areas include: active transportation; planning and policy; security and counterterrorism; sustainable transportation and land use; transit and passenger rail; transportation engineering; transportation finance; transportation technology; and workforce and labor. MTI research publications undergo expert peer review to ensure the quality of the research.

Education and Workforce Development

To ensure the efficient movement of people and goods, we must prepare the next generation of skilled transportation professionals who can lead a thriving, forward-thinking transportation industry for a more connected world. To help achieve this, MTI sponsors a suite of workforce development and education opportunities. The Institute supports educational programs offered by the Lucas Graduate School of Business: a Master of Science in Transportation Management, plus graduate certificates that include High-Speed and Intercity Rail Management and Transportation Security Management. These flexible programs offer live online classes so that working transportation professionals can pursue an advanced degree regardless of their location.

Information and Technology Transfer

MTI utilizes a diverse array of dissemination methods and media to ensure research results reach those responsible for managing change. These methods include publication, seminars, workshops, websites, social media, webinars, and other technology transfer mechanisms. Additionally, MTI promotes the availability of completed research to professional organizations and works to integrate the research findings into the graduate education program. MTI's extensive collection of transportation-related publications is integrated into San José State University's world-class Martin Luther King, Jr. Library.

Report 25-16

An Ambient NO_X Reduction Reactor System with and without Forced Air

Hamid Rahai, PhD

Ryan Moffit

Komal Gada

Jermey Bonifacio, PhD

July 2025

A publication of the
Mineta Transportation Institute
Created by Congress in 1991

College of Business
San José State University
San José, CA 95192-0219

TECHNICAL REPORT DOCUMENTATION PAGE

1. Report No. 25-16	**2. Government Accession No.**	**3. Recipient's Catalog No.**	
4. Title and Subtitle An Ambient NO_X Reduction Reactor System with and without Forced Air		**5. Report Date** July 2025	
		6. Performing Organization Code	
7. Authors Hamid Rahai, PhD Ryan Moffit Komal Gada Jermey Bonifacio, PhD		**8. Performing Organization Report** CA-MTI-2442	
9. Performing Organization Name and Address Mineta Transportation Institute College of Business San José State University San José, CA 95192-0219		**10. Work Unit No.**	
		11. Contract or Grant No. CA-MTI-2442	
12. Sponsoring Agency Name and Address State of California SB1 2017/2018 Trustees of the California State University Sponsored Programs Administration 401 Golden Shore, 5th Floor Long Beach, CA 90802		**13. Type of Report and Period Covered**	
		14. Sponsoring Agency Code	
15. Supplemental Notes 10.31979/mti.2025.2442			

16. Abstract

Ambient nitrogen oxide (NO_X) is one of the main ingredients involved in the formation of ground-level ozone (smog), which contributes to global warming and the formation of particulates in the atmosphere and causes respiratory illnesses, especially in children, older adults, and people with lung diseases. Investigations on adding titanium dioxide (TiO_2) nanoparticles to the paint used on concrete surfaces such as buildings and its potential in reducing ambient NO_X concentration have provided opportunities for the research and development of methods for passive control and filtration of the ambient NO_X. The present research used numerical geometrical optimization to identify an optimized surface geometry of half-stepped cylinders for increasing air recirculation and residence time for maximum ambient NO_X reduction. The optimized surface was painted with titanium-infused paint and tested for NO_X reduction according to ISO 22197-1 standard. Results showed a maximum of 11.5% increase in NO_2 formation for an optimized surface compared with the result for the untextured smooth surface, with an estimated NO_X reduction of approximately 15%. The results provided guidelines for developing a catalyst system for reducing ambient NO_X when UV light is present. These results demonstrate potential of using paint infused with titanium to help reduce NO_X and thus reduce smog, which harms people and the environment.

17. Key Words Air quality management, air pollution, infrastructure, greenhouse gases, global warming.	**18. Distribution Statement** No restrictions. This document is available to the public through The National Technical Information Service, Springfield, VA 22161.		
19. Security Classif. (of this report) Unclassified	**20. Security Classif. (of this page)** Unclassified	**21. No. of Pages** 31	**22. Price**

Form DOT F 1700.7 (8-72)

DOI: 10.31979/mti.2025.2442

Mineta Transportation Institute
College of Business
San José State University
San José, CA 95192-0219

Tel: (408) 924-7560
Fax: (408) 924-7565
Email: mineta-institute@sjsu.edu

transweb.sjsu.edu/research/2442

ACKNOWLEDGMENTS

Funding for this research was provided by the California State University Transportation Consortium through the State of California's Senate Bill 1, the Road Repair and Accountability Act of 2017.

The authors thank Lisa Rose and Editing Press for editorial services, as well as MTI staff Project Assistant Rajeshwari Rajesh and Graphic Design Assistant Katerina Earnest.

CONTENTS

Acknowledgments vi

List of Figures viii

List of Tables ix

Executive Summary 1

1. Introduction 2

2. Methodology 4

2.1 Numerical Optimization 4

2.2 Experimental Verification 5

2.3 Forced Air Experimentation 8

3. Results and Discussions 9

3.1 Numerical Results 9

3.2 Experimental Results 11

4. Summary and Conclusions 16

Bibliography 17

About the Authors 20

List of Figures

Figure 1. A V-Grooved Riblet 3

Figure 2. The Optimization Processes. 4

Figure 3. The Aligned Half-Stepped Cylinder Sheet 5

Figure 4. The Offset Half-Stepped Cylinder Sheet 5

Figure 5. The Experimental Setup 6

Figure 6. The Test Setup 7

Figure 7. An Optimized Row of Half-Stepped Cylinders 9

Figure 8. Offset Rows of Half-Stepped Cylinders 10

Figure 9. Velocity Vector Through the Optimized Half-Stepped Cylinders 11

Figure 10. Test Samples from Left to Right: Smooth, 5X Parallel, 5X Perpendicular, 2X Parallel, 2X Perpendicular 11

Figure 11. NO_2 Formed for the ISO-Standard Test Condition 12

Figure 12. NO_2 Formation with the Forced Air 14

Figure 13. Variations of NO_2 with Time for Forced Air at a Velocity of 1 m/s 15

LIST OF TABLES

Table 1. The Composition of the TiO_2 Coating 7

Table 2. Paints Tested 8

Table 3. NO_2 Concentration with Standard ISO Condition 13

Table 4. NO_2 Formation for the Forced-Air System 14

Table 5. Comparison of NO_2 Formation for the Forced-Air and the ISO-Standard Conditions 15

Executive Summary

Numerical optimization was performed to develop optimized staggered wave surfaces in the form of half-stepped cylinders for the development of reactor surfaces covered with titanium dioxide (TiO_2) infused paint for increased reduction in ambient NO concentration. While the numerical results showed increased air recirculation over the optimized surface, due to the limitations in surface textured fabrication, the experimental verifications of the numerical results were conducted using surfaces with textured geometries scaled uniformly to 5 times (5X) of the optimized geometries. The wave surfaces were tested at two orientations of parallel and perpendicular to the flow direction. They were initially covered with 7% by-weight TiO_2-infused paint and tested according to the ISO22197-1 standard. Results indicated 5.3% and 11.5% increases in NO_2 formation for 5X-parallel and 5X-perpendicular surfaces, respectively, when compared with the result for the untextured smooth surface, which corresponds to estimated NO_X reductions of approximately 7% and 15%.

1. Introduction

Disadvantaged populations have traditionally borne a greater pollution burden than other communities, and sensitive populations within and around these communities are more vulnerable to the effects of pollution than other populations. Trades and goods movements are major components of California's economy, with adverse environmental impacts, especially on disadvantaged communities. According to the California Air Resources Board (CARB), high levels of air pollution are present in proximity to freeways and high-traffic roadways and can negatively impact communities within 1000 ft of these roads. Studies (Rahai, 2008; Rahai and Sciortino, 2012) on the diffusion of particulate matter (PM) from the passage of diesel locomotives near the Port of Los Angeles have shown high concentrations of diesel particulates up to nearly 200 ft from the railroad and increased PM concentration near the structures in these areas.

Senate Bill 1000 (SB 1000) requires cities and counties to include policies and objectives for reducing pollution exposure, improving air quality, engaging the community in the public decision-making process, and meeting the needs of disadvantaged communities in their plans. Senate Bill 535 (SB 535) directs 25% of the proceeds from the greenhouse gas reduction fund to projects that benefit disadvantaged communities, and Assembly Bill 1550 (AB 1550) requires that the fund be spent on projects within these communities. The disadvantaged communities are identified by the CalenviroSreen model.

Nitrogen oxides (NO_X) are greenhouse gases, and reductions in the tailpipe and ambient NO_X improve climate change. Ambient NO_X is one of the main ingredients involved in the formation of ground-level ozone (smog), which causes respiratory illnesses—especially in children, older adults, and people with lung diseases—and contributes to global warming and the formation of particulates in the atmosphere. Heavy-duty diesel vehicles (HDVs) are responsible for more than 70% of NO_X emissions of on-road vehicles in California.

Investigations of the addition of titanium dioxide (TiO_2) nanoparticles to paint and its potential in reducing ambient NO_X concentration have provided opportunities for research and development of methods for passive control and filtration of the ambient NO_X. Previous investigations (Dylla et al., 2010; Hassan et al., 2010; Dylla et al. 2011; Allen et al., 2008; Zhao et al., 2003; Choi et al., 2002; Cassar et al., 2003; Guo et al., 2015; Janus et al., 2019; Yu et al., 2020; Wang et al., 2018) have shown that the surface coating of concrete walls with TiO_2 in the form of a cementitious ultra-thin surface layer reduces ambient NO concentration and application of paint infused with TiO_2 to building surfaces has shown antifouling performance and ambient NO_X reduction by 30%–40%. The addition of TiO_2 to cement road materials has shown up to an 80% reduction in ambient NO_X. The behavior of TiO_2 changes when a mixture of NO and NO_2 is present, and a higher NO_2/NO_X ratio negatively impacts the effectiveness of the photocatalytic process. The maximum photodegradation rate was found at 25% relative humidity.

A study on the effects of different levels of irradiation and humidity on the NO_X reduction effectiveness of surfaces painted with paint-infused TiO_2 has shown that, even with low levels of irradiation and for a range of humidity levels, the TiO_2-infused paint could still reduce NO_X concentration (Song et al., 2020).

These studies have indicated that surface texture, the distribution of TiO_2 on the surface, and residence time (exposure time) play major roles in the effectiveness ofTiO_2-infused paint for controlling ambient NO_X.

Increasing residence time requires development of a surface texture where air could be trapped, increasing the time for chemical reaction and reducing NO_X concentration. Within an urban canopy, flow around structures ranged from very low Reynolds numbers of natural convection to highly turbulent flows, and surface textures impact flow conditions at and near the surface within the boundary layer. There have been extensive investigations of how riblets affect laminar and turbulent boundary layers (Bushnell & Hefner, 1990; Gad-el-Hak, 2000; García-Mayoral & Jiménez, 2011; Sareen et al., 2014; Khader & Sayma, 2018; Raayai-Ardakani & McKinley, 2019; Houshmand et al., 1983). Figure 1 shows a typical riblet.

Figure 1. A V-Grooved Riblet (Raayai-Ardakani & McKinley, 2019)

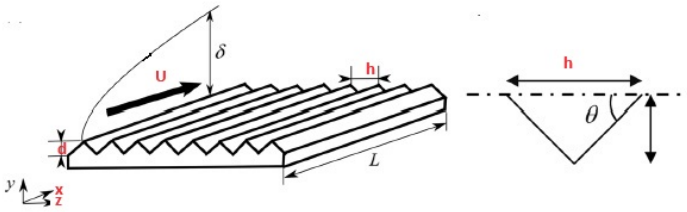

In a laminar boundary layer over a ribbed surface, the flow inside the grooves is increasingly retarded, creating a layer of slow-moving fluid and resulting in lower shear stress inside the grooves, especially at the base of the grooves. This shear stress is lower than the corresponding shear stress for a smooth flat plate boundary layer. Increasing the riblets' aspect ratio (h/d) increases the thickness of the viscous boundary layer, and the axial vorticity within the groove decreases with increasing length of the groove. These results indicate that creating a layer of slow-moving fluid and increasing the thickness of the viscous boundary layer could increase the residence time and meet our objective of higher ambient NO_X reductions.

The present research used geometrical optimization to identify an optimized surface geometry of half-stepped cylinders for increasing air recirculation and residence time for maximum ambient NO_X reduction. The optimized surface was painted with titanium-infused paint and tested for NO_X reduction according to ISO 22197-1 standard (Houshmand et al., 1983).

2. Methodology

2.1 Numerical Optimization

ANSYS OptiSlang's Adaptive Metamodel of Optimal Prognosis (AMOP), in conjunction with the Design of the Experiment (DOE), was used for the optimization process. CFD ANSYS Fluent was used for all the simulations. Figure 2 shows the optimization process. DOE is a systematic approach to generating the desired number of design points based on the minimum and maximum values set for each parameter. These design points form the basis of initial training data in the Metamodel of Optimal Prognosis (MOP) machine learning algorithm. A metamodel is a model of models such that a single metamodel can provide surface responses, sampling data, and filtration of variables for Reduced Order Modeling (ROM), for accurate prediction.

MOP surveys the data, calculates the Coefficient of Prognosis (CoP) values, and compares them using cross-validation. MOP then selects the best metamodel and parameters with their contributions, which identifies the parameters with the most impact. Using these results, DOE is redefined, and a new simulation is conducted. The process continues until the optimum design parameters and the best possible output for the given conditions are achieved.

The numerical optimization and simulations were performed using the CSULB High-Performance Computing (HPC) in conjunction with ANSYS OptiSlang software and Fluent Solver.

Figure 2. The Optimization Processes

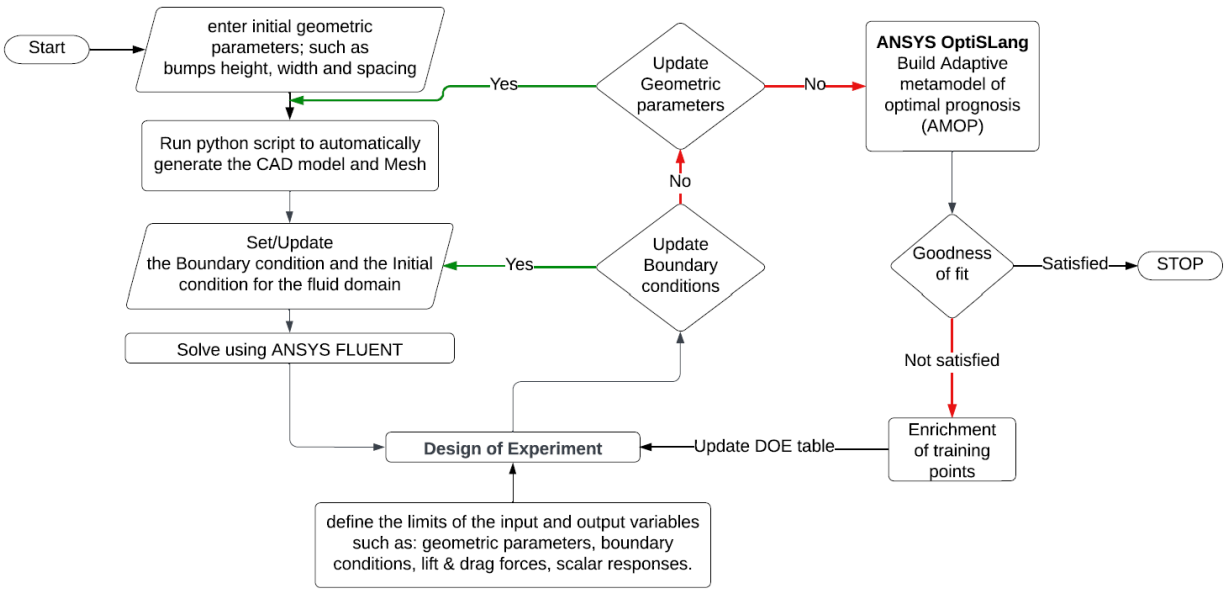

The major geometrical dimensions for optimization were the radius (r) and width (w) of the step and the spacing (s) between adjacent steps. The numerical optimization was focused on optimizing these parameters for maximum recirculation. The optimization was performed in two configurations: (1) the stepped cylinders were aligned, similar to ridges (Figure 3) and (2) offset half-stepped cylinders (Figure 4). The CFD simulations were performed at zero pressure gradients on a flat plate with the optimized half-stepped cylinder surface.

Figure 3. The Aligned Half-Stepped Cylinder Sheet

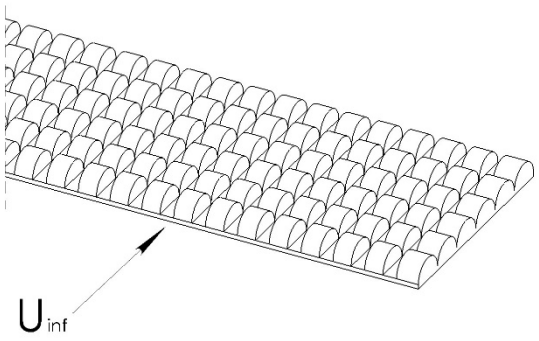

Figure 4. The Offset Half-Stepped Cylinder Sheet

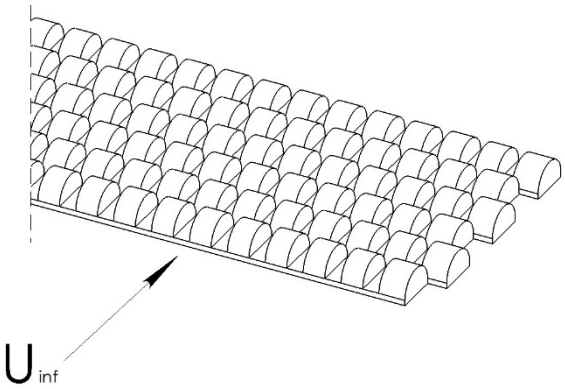

2.2 Experimental Verification

The experiments were conducted according to International Standard ISO 22197-1 (2007). Figures 5 and 6 show the experimental setup. The ISO Reactor is a small chamber, a plexiglass box with inside dimensions of 28 cm in length, 14 cm in height, and 14 cm in width. The top surface is an access door allowing the placing of the sample on a flat-plate sample holder. The sample holder has a 25 mm width and 2 mm depth cutout at the mid-section spanning the length of the box at the mid-height. The box has inlet and outlet supply lines aligned with the flat-plate sample holder. For all tests, except the top surface that was exposed to UV light, the other sides were covered with black opaque paper to minimize outside light exposure. The samples have

projected surface dimensions of 5 cm by 10 cm (50 cm^2 area) and 5 mm thickness fitted tightly into the sample holder.

The light source was an Everbeam 365nm 50W LED Black Light. The distance Y between the light source and the reactor was adjusted to maintain a nearly 10 W/m^2 irradiance at the sample surface. The level of radiation was confirmed with an AMTAST UV340B light meter with a wavelength of 290–390 nm with an accuracy of ±(4% FS+2digit) for a range to 40 mW/cm^2.

A Zynect Air-Quality Egg was used for monitoring temperature, humidity, and NO_2 with the operating ranges of -40˚C–125˚C, 0–100%, and up to 1 ppm, respectively. The uncertainties in temperature, humidity, and NO_2 measurements were respectively ±0.1˚C, ±1.5%, and ±16 ppb for ≤ 150 ppb and ±10% for > 150 ppb. Data monitoring and collection were performed using a mini PC.

Figure 5. The Experimental Setup

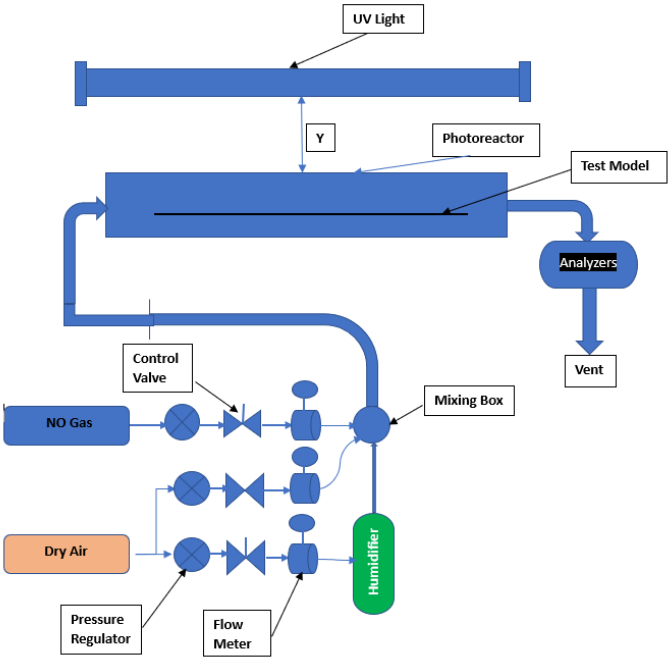

Figure 6. The Test Setup

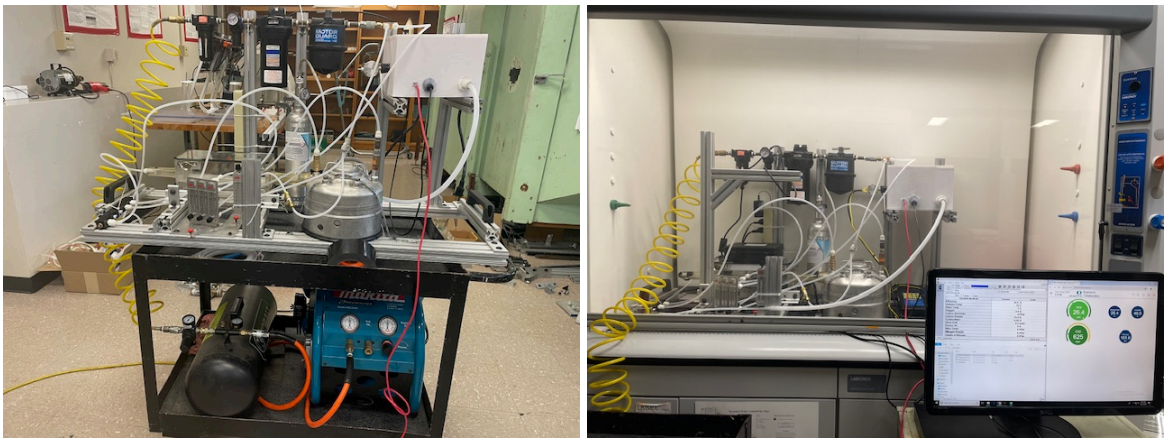

A ProJet 6000HD-3D printer was used to print a baseline flat surface sample and samples with various scaled of the optimized geometry. The samples' dimensions were approximately 50 mm wide, 100 mm long, and 5 mm thick. The samples were tested for different orientations, the printed texture being parallel or perpendicular to the flow direction. The samples were exposed to the UV light at an irradiance of 10 W/m^2 for 16 hours to decompose any residual organic matter on the surface before the tests.

Initially, we prepared a TiO_2 coating composition according to Table 1 (Bushnel & Hefner, 1990). However, we had difficulty maintaining a highly mixed solution, even with an ultrasonic mixer. Then the decision was made to try various water-based paints with the addition of 2% weight-reinforced TiO_2. Table 2 shows the paint specifications with the addition of TiO_2 concentration. The mixture was mixed thoroughly before application. The coating was applied with an airbrush, and then the samples were allowed to dry in an oven at 50°C for 24 hours. Care was taken to maintain the same thickness on all samples. The samples were weighed again, and the new weights were recorded.

Table 1. The Composition of the TiO_2 Coating

Composition of TiO_2 Coating by Weight	
TiO_2	1.75%
Silicon Compound	5.6%
Ethanol	41.6%
Water	51.05%

Table 2. Paints Tested

Paint Brand	Paint % Weight	Initial TiO_2 Composition	Total TiO_2 % Weight
Acrylic	98	2%	7%

The tests were conducted according to the following procedure:

1. The baseline sample was placed in the photoreactor, and the light source distance was adjusted to maintain an irradiance of 10 W/m^2 at the sample location. The light source was then turned off.

2. The standard NO gas with a volume fraction of 100 µl/l and flow rate of 0.1 l/min was mixed with dry air at 1 l/min and wet air at nearly 40% RH at 2 l/min. The mixed gas from the mixing box was fed to the photoreactor. The flow is maintained for 30 minutes, and the volume fraction of NO_2, temperature, and humidity were recorded. The flow rate was to maintain an RH ±3% and temperature of 25°C ±10%.

3. Commence irradiation of the sample and continue measuring NO_2, RH, and temperature for 5 hours.

4. Stop irradiation and continue recording parameters as in step 3 for 30 minutes.

2.3 Forced Air Experimentation

To assess the effects of increased air movement on the photochemical conversion, selective samples were tested with an air velocity of 1 m/s aligned with the optimization of the numerical results. The same setup as before was used with increased volume flow rate to have a speed of 1 m/s over the sample's surface while NO concentration and humidity were maintained constant. With the sample in place, the test procedure was according to the following steps:

1. Start the dry and wet air and maintain flow for 30 minutes.

2. Turn the NO gas on for 10 minutes without the UV light on.

3. Turn the UV light on for 2 hours, while continuously collecting data.

4. Turn the light and NO gas off and run dry and wet air for 30 minutes.

3. Results and Discussions

3.1 Numerical Results

The numerical optimizations were performed at a mean velocity of 1 m/s to obtain the design parameters for maximum recirculation. Figure 7 shows the dimensions of the optimized geometries for one row of the half-stepped cylinders. The optimized dimension between the crest and trough was 0.655 mm and between the peak-to-peak half-stepped cylinder was 0.650 mm. To increase circulation, the rows of the half-stepped cylinders were offset by 0.38125 mm peak-to-peak to force the gas through and over the cylinders, increasing the residence time for a maximum NO_X conversion (Figure 8).

Figure 9 shows the velocity vectors through the optimized half-stepped cylinders. The results show increased recirculation through the cavity. The corresponding circulations over the entire surface for the smooth and the optimized surfaces are respectively 0.389 m^2/s and 0.598 m^2/s, which indicates that the circulation for the optimized surface has increased by more than 53% when compared with the circulation for the smooth surface. The increase in circulation is associated with increased residence time and should result in a higher NO_X conversion.

Figure 7. An Optimized Row of Half-Stepped Cylinders

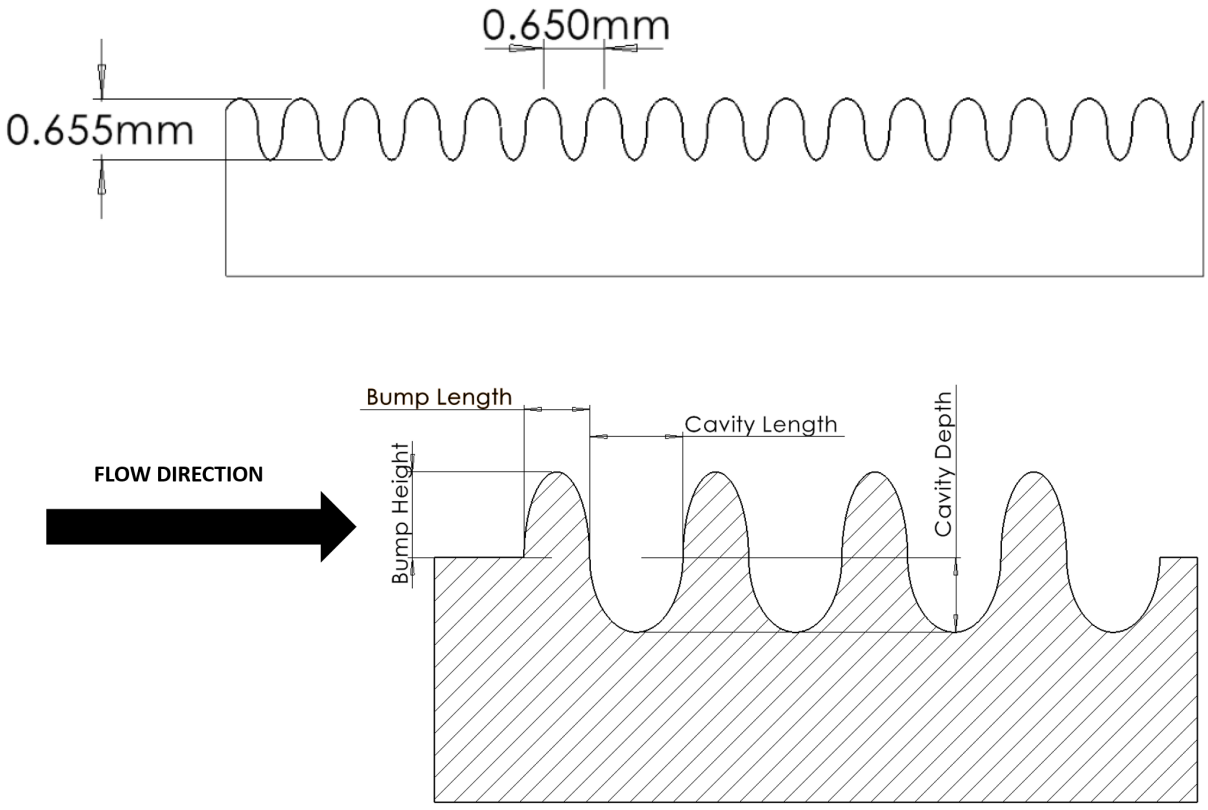

Figure 8. Offset Rows of Half-Stepped Cylinders

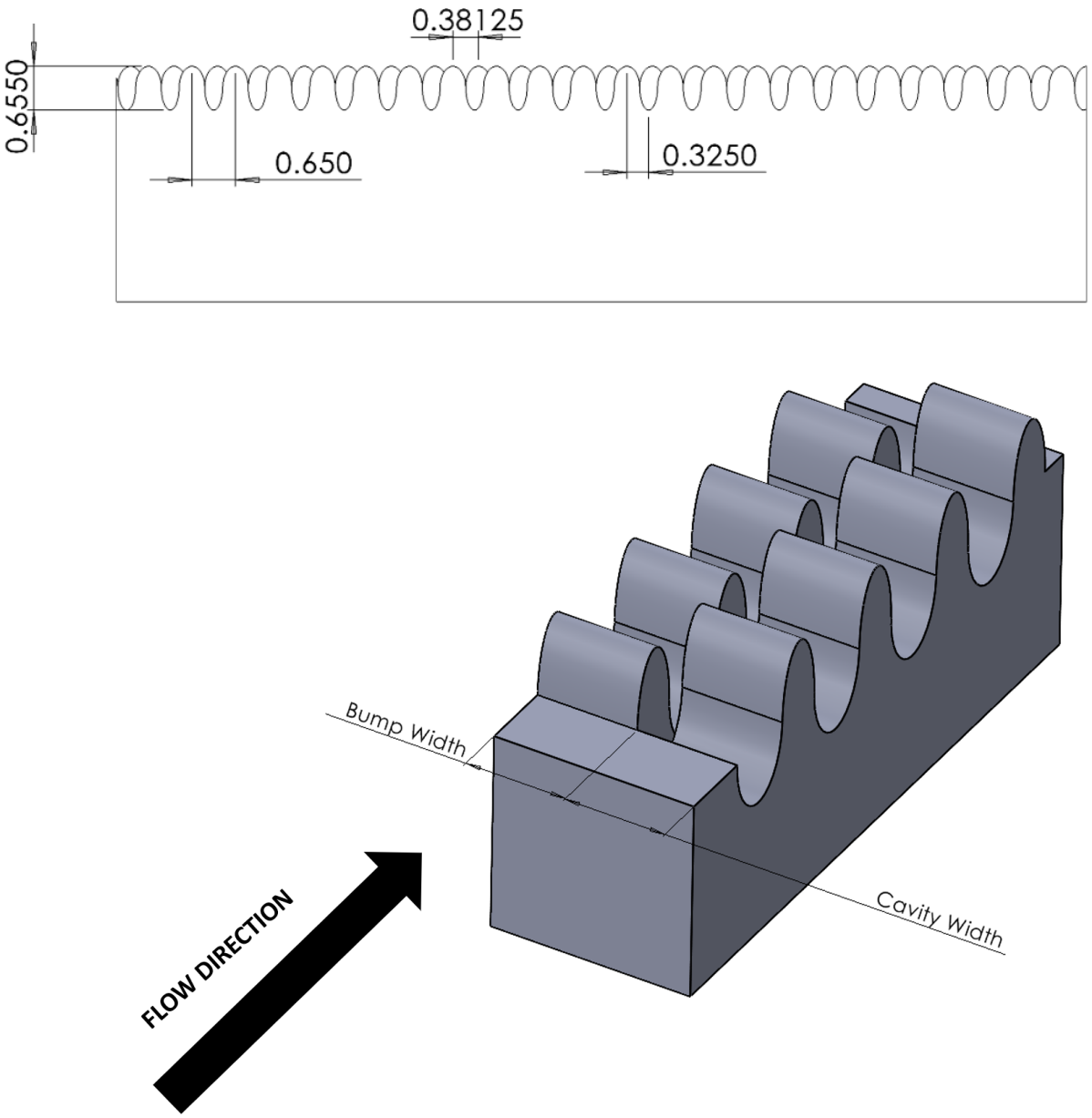

Figure 9. Velocity Vector Through the Optimized Half-Stepped Cylinders

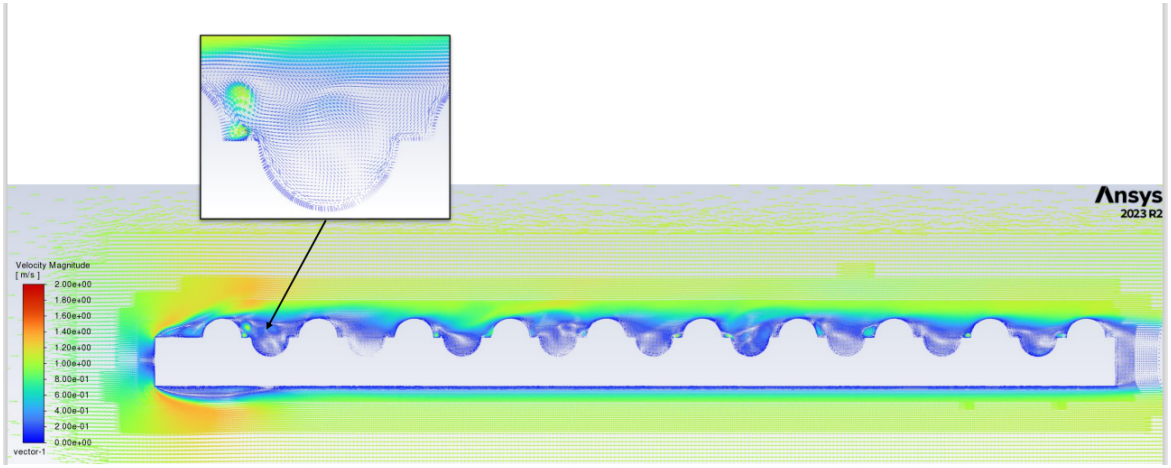

3.2 Experimental Results

3.2.1 ISO-Standard Test Results

Due to the printer's limitations, we could not print the exact textured surface based on the dimensions from the numerical optimization. The nearest scale that was printed was twice the scale (2X) texture. We also proceeded with testing the 5X scales to assess the effects of a larger scaling on NO_X conversion. Figure 10 shows the samples tested.

Figure 10. Test Samples from Left to Right: Smooth, 5X Parallel, 5X Perpendicular, 2X Parallel, 2X Perpendicular. The Direction of the Gas is from Top to Bottom

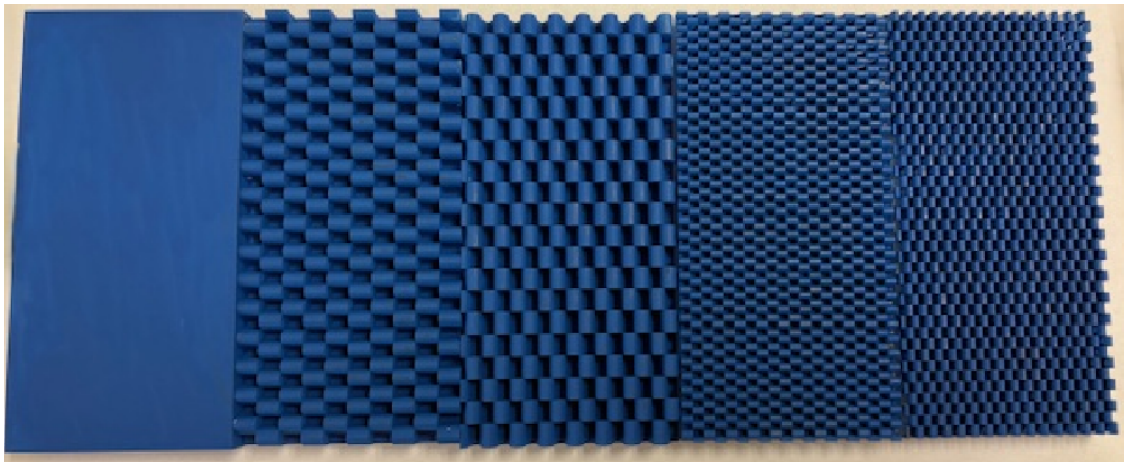

Figure 11 shows the changes in nitrogen dioxide (NO_2) concentration for the flat and 5X samples with 7% TiO_2-infused paint under ISO-standard testing conditions. For the flat surface, the nitrogen NO_2 concentration decreases initially before it increases to a maximum of 0.0844 ppm at the light-off. For the 5X-parallel sample, with the light on, the maximum NO_2 concentration is 0.089 ppm just before the light off, and for the 5X-perpendicular, the maximum is 0.093 ppm before it decreases to 0.089 at the light off. Table 1 shows the total NO_2 increase by the test pieces between the light on and off. The increase in NO_2 concentration is 5.3% for the 5X parallel and 11.5% for the 5X perpendicular. Previous investigation (Song et al., 2020) has shown that a 13.6% in NO_2 production is associated with respectively 35.6% and 21.6% reduction in NO and NO_X concentrations. Although our sensor did not measure NO concentration directly to accurately estimate the increase in NO_X reduction, based on this previous investigation, for the 5X textured surfaces, we can infer that the increase in NO_X reduction would be between 7% and 15%.

Figure 11. NO_2 Formed for the ISO-Standard Test Condition

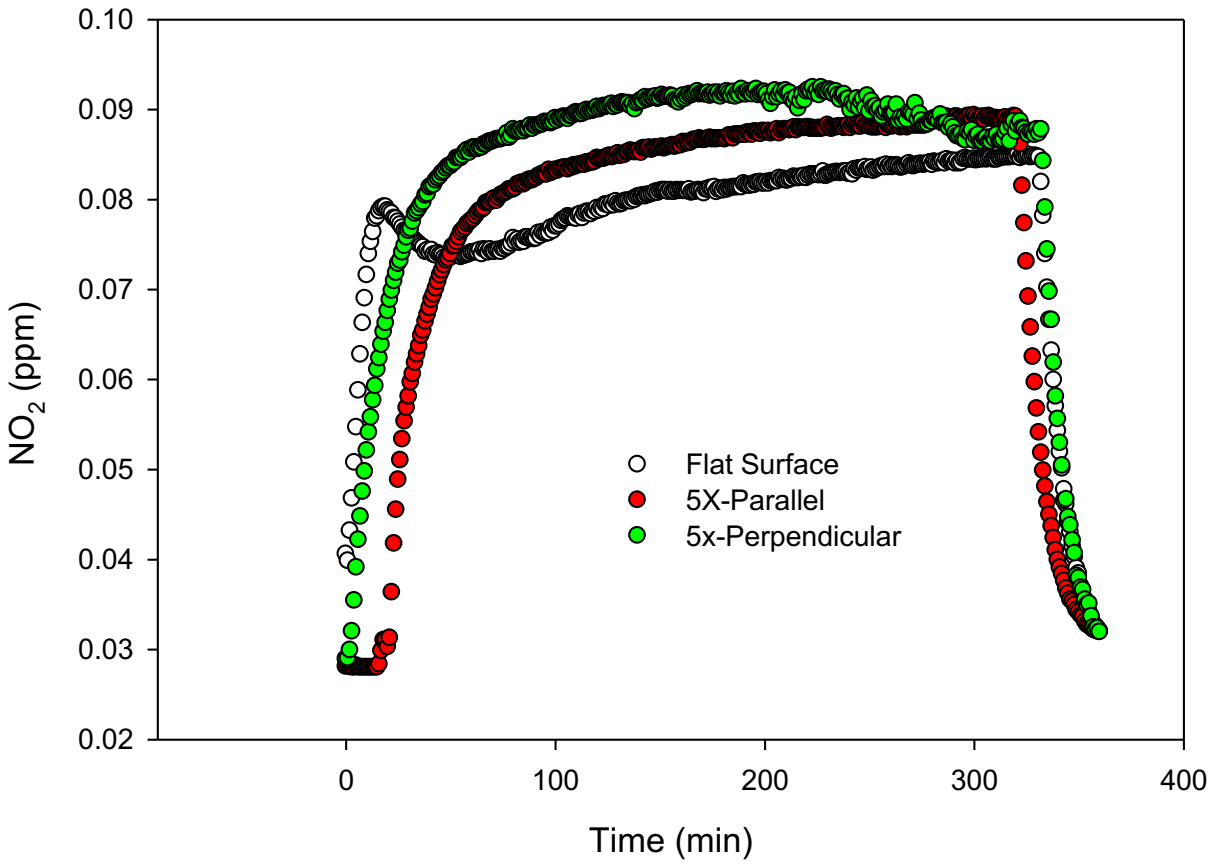

Table 3. NO_2 Concentration with Standard ISO Condition

	Flat	5X Parallel	5X Perpendicular
μmol	2.89	3.04	3.22
% Increase		5.2	11.4

3.2.2. Forced Air

As mentioned before, the geometrical dimensions for the optimized staggered sinusoidal wave surfaces were too small for our printer to fabricate, and testing the surfaces with 2X dimensions did not result in a significant change in NO_X reduction under ISO-standard testing conditions. Only the 5X configurations increased the contact between the layer of air near the surface and the samples for increased NO_2 formation.

Further increasing NO_X conversion without modifying the chemical reaction rates requires a higher flow rate to increase the volume of air in contact with the reactive surface. In addition, the numerical optimization results were conducted at a mean speed of 1 m/s over the surface, which is significantly higher than the gas-air mixture speed of the ISO-standard test condition. To meet the condition prescribed in the numerical optimization, the volume flow rates of the dry and wet air were increased by 5 times while the NO concentration remained the same, resulting in a NO concentration of 0.2 ppm. Figure 12 shows the corresponding results for the increased flow condition. The level of NO_2 formation is reduced for all cases when compared with the standard ISO test results, which would be expected from the decrease in incoming NO concentration. However, the flat surface results now show a higher NO_2 formation as compared with the 5X surfaces with the results for the parallel surface being higher than the perpendicular surface. Table 4 shows the NO_2 concentration. The reduction in NO_2 formation for 5X parallel and perpendicular surfaces are respectively 15% and 24% when compared with the corresponding result for the flat surface. Here we postulate that with increased air speed to 1 m/s, the contact between the textured surfaces and the air is reduced due to the formation of the cavities resulting in a lower reaction and less NO_2 formation.

Figure 12. NO_2 Formation with the Forced Air

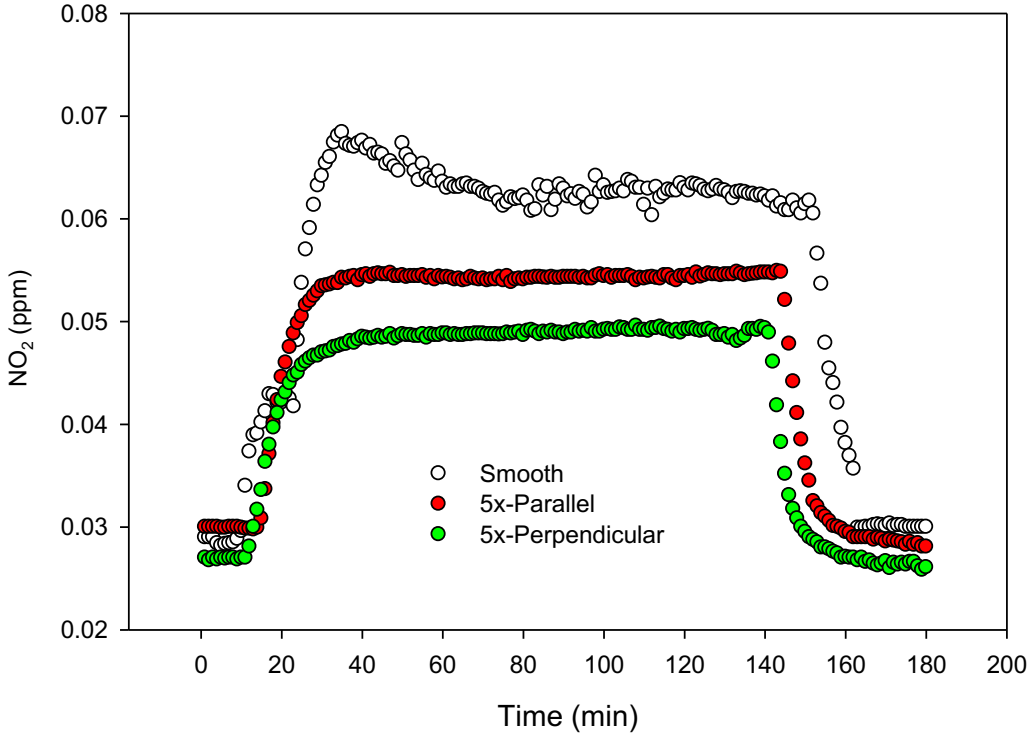

Table 4. NO_2 Formation for the Forced-Air System

	Flat	5X Parallel	5X Perpendicular
µmol	5.1	4.33	3.85
% Reduction		15	24.5

The above results are for supplied NO gas at 0.2 ppm concentration. To compare the forced-air and ISO-standard results, the above results need to be adjusted for 1 ppm supplied NO. Previous investigation (Song et al., 2020) has shown a four-fold change in ppm of NO results in a two-fold change in NO_2 formation. Table 5 shows the comparisons of the forced-air and ISO-standard results. The data has been adjusted for a one-hour test. For the forced air, the increase in NO_2 formation is 4.4-fold for the smooth surface and 3.54-fold and 3.0-fold for 5X-parallel and 5X-perpendicular surfaces, respectively. These results indicate that with the forced-air system, a much higher level of NO_X reduction could be obtained and mitigating the challenge associated with manufacturing the optimized dimensions of the staggered sinusoidal wave surface could increase the recirculation and residence time at this speed and thus achieving a higher NO_X reduction.

Table 5. Comparison of NO_2 Formation for the Forced-Air and the ISO-Standard Conditions

µmol/hr	Flat	5X Parallel	5X Perpendicular
ISO Standard	0.58	0.61	0.64
Forced Air	2.55	2.16	1.925
Ratio	4.4	3.54	3.0

Figure 13. Variations of NO_2 with Time for Forced Air at a Velocity of 1 m/s

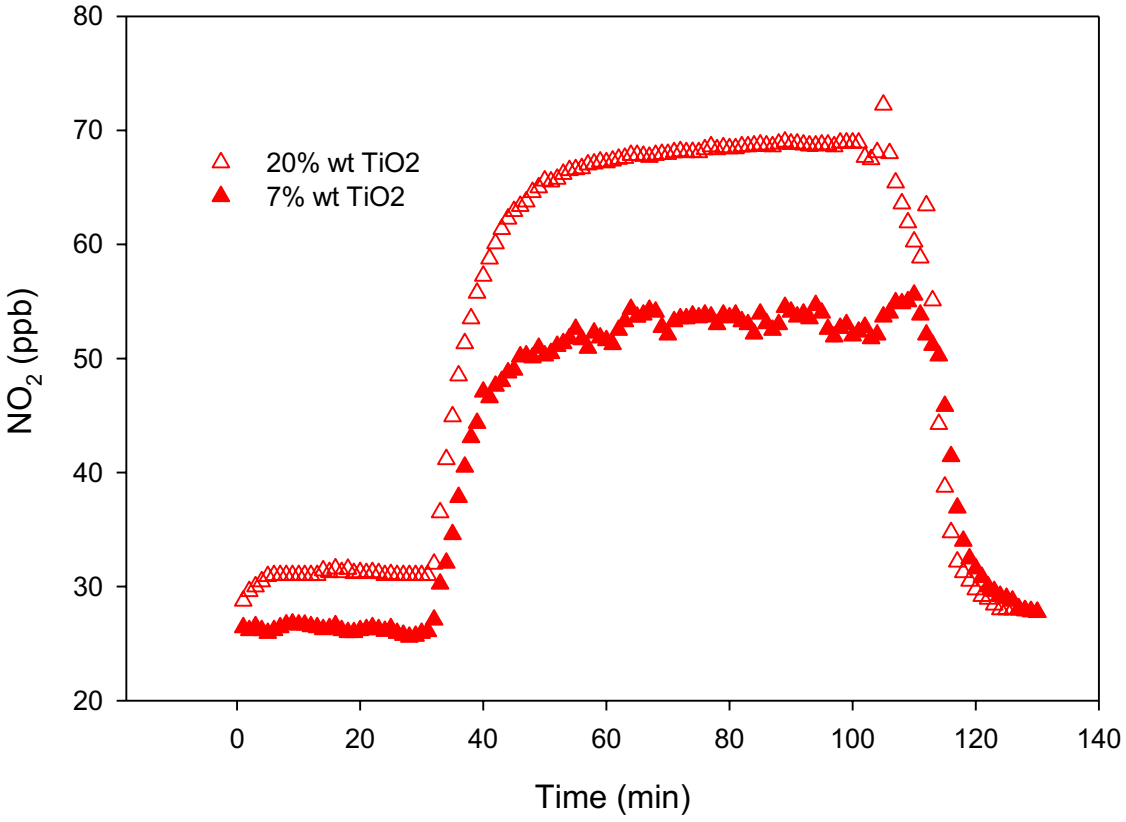

4. Summary and Conclusions

Numerical optimization was used for the development of optimized staggered sinusoidal surfaces for an ambient NO_X reduction reactor. For experimental verifications, the surfaces were fabricated at five times the optimized geometries and tested at two orientations of the textured surface, being parallel and perpendicular to the flow direction (5X-parallel and 5X-perpendicular). The surfaces were initially painted with 7% TiO_2-infused paint and tested using the ISO 22197-1-2007 standard. Results indicated a 5.3% and 11.5% increase in NO_2 for surfaces being respectively at perpendicular and parallel orientations. when compared with the corresponding result for the smooth surface. These increases correspond to estimated NO_X reductions of 7% and 15%. The 5X parallel surface was also tested for increased TiO_2 concentration from 7% to 20%, and results showed a 25% increase in NO_2 formation.

These surfaces were then tested with a forced gas-air mixture at 1 m/s, without changing the incoming NO concentration, and results indicated increases in NO_2 formation for smooth, 5X-parallel, and 5X-perpendicular by 4.4, 3.54, and 3.0 folds, respectively, when compared with the corresponding results from the ISO-standard tests. While the forced-air approach showed a substantial increase in NO_2 formation and thus NO_X reduction, we postulate that, at this speed, flow over the textured surfaces forms micro-cavities resulting in reduced recirculation and contact between the incoming gas and the surface and thus a lower NO_2 formation when compared with the results for the smooth surface.

Bibliography

Allen, N. S., Edge, M., Verran, J., Stratton, J., Maltby, J., & Bygott, C. (2008). Photocatalytic titania-based surfaces: Environmental benefits. *J. of Polymer Degradation and Stability*, *93*, 1632–1646.

Bushnel D. M., & Hefner J. N. (Eds.). (1990). *Viscous Drag Reduction in Boundary Layers*. AIAA.

Cassar, L., Pepe, C., Tognon, G., Guerrini, G. L., & Amadelli, R. (2003). White cement for architectural concrete, possessing photocatalytic properties. In *Proceedings of the 11th International Congress on the Chemistry of Cement, Durban, South Africa, May 11–16, 2003*. https://iccc-online.org/fileadmin/gruppen/iccc/proceedings/ICCC11_2003.pdf

Choi, Y. J., Park, J. Y., Lee, S. J., Huh, N. I., & Kim, H. J. (2002). A fundamental study on the properties of NO_X removal on cement mortar with TiO_2 powder as photocatalyst. *J. Archit. Instit. Korea Struct. Constr.*, *18*, 43–50.

Dylla, H., Hassan, N. M., Mohammad, L., & Rupnow, T. (2010). Evaluation of the environmental effectiveness of titanium dioxide photocatalyst coating for concrete pavements. *Transp. Res. Rec.*, *2164*(1), 46–51.

Dylla, H., Hassan, M. M., Schmidt, M., Rupnow, T., & Mohammad, L. N. (2011) Laboratory investigation of the effect of mixed nitrogen dioxide gases on titanium dioxide photocatalytic efficiency in concrete pavements. *J. of Materials in Civil Engineering*, *23*, 1087–1093.

Gad-el-Hak, M. (2000). *Flow Control, Passive, Active, and Reactive Flow Management*. Cambridge University Press.

García-Mayoral, R., & Jiménez, J. (2011). Drag reduction by riblets. *Philos. Trans. R. Soc., A. 369*, 1412–1427.

Guerrini, G. L., Beeldens, A., Crispino, M., D'Ambrosio, G., & Vismara, S. (2012). Environmental benefits of innovative photocatalytic cementitious road materials. In *Proceedings of the 10th International Conference on Concrete Pavements, Quebec City, QC, Canada, July 8–12, 2012*. https://www.concretepavements.org/conference-proceedings/

Guo, M.-Z., Maury-Ramirez, A., & Poon, C. S. (2015). Photocatalytic activities of titanium dioxide incorporated architectural mortars. *Build. Environ.*, *94*, 395–402.

Hassan, M. M., Dylla, H., Mohammad, L., & Rupnow, T. (2010). Evaluation of the durability of the titanium dioxide photocatalyst coating for concrete pavement. Constr. Building Mater., 24(8), 1456–1461.

Houshmand, D., Youngs, R., Wallace, J., & Balint, J. (1983). An experimental study of changes in the structure of a turbulent boundary layer due to surface geometry changes. *AIAA Paper No. 83-0230*.

International Standard. (2016, November 11). *Fine ceramics (advanced ceramics, advanced technical ceramics) – Test method for air-purification performance of semiconducting photocatalytic materials – Part 1: Removal of nitric oxide*. Second edition, ISO 22197-1.

Janus, M., Madraszewski, S., Zajac, K., Kusiak-Nejman, E., Morawski, A. W., & Stephan, D. (2019). Photocatalytic activity and mechanical properties of cements modified with TiO_2/N. *Materials*, *12*, 3756.

Khader, M., & Sayma, A. (2018). Drag reduction within radial turbine rotor passages using riblets. *Proc. Inst. Mech. Eng.*, *Part E*.

Raayai-Ardakani, S., & McKinley, G.H. (2019). Geometric optimization of riblet-textured surfaces for drag reduction in laminar boundary layer flows. *Phys. Of Fluids*, *31*, 053601.

Rahai, H. (2008, February). Development of an exposure model for diesel locomotive emissions near the Alameda Corridor. *METRANS Final Technical Report*. AR 05-03 Final_0_0.pdf (metrans.org)

Rahai, H., & Sciortino, A. (2012, April). The effects of distortion on trajectory of diesel particulate matter (PM) from mobile sources. *METRANS Final Report*. 10- 20_Rahai-Scortino_final_0_0.pdf (metrans.org)

Sareen, A., Deters, R. W., Henry, S. P., & Selig, M.S. (2014). Drag reduction using riblet film applied to airfoils for wind turbines. *J. Sol. Energy Eng.*, *136*, 021007.

Song, Y. W., Kim, M. Y., Chung, M. H., Yang, Y. K., & Park, J. C. (2020). Nox-reduction performance test of TiO_2 paint. *Molecules*, *25*, 4087; doi:10.2290/molecules25184087.

Wang, H., Jin, K., Dong, X., Zhan, S., & Liu, C. (2018). Preparation technique and properties of nano-TiO_2 photocatalytic coatings for asphalt pavement. *Appl. Sci.*, *8*, 2049.

Yu, H., Dai, W., Qian, G., Gong, X., Zhou, D., Li, X., & Zhou, X. (2020). The NO_X degradation performance of nano-TiO_2 coating for asphalt pavement. *Nanomaterials*, *10*, 897.

Zhao, J., & Yang, X. (2003). Photocatalytic oxidation of indoor air purification: A literature review. *Build Environ.*, *38*(5), 645–654.

About the Authors

Hamid Rahai, PhD

Dr. Hamid Rahai is a professor in the Department of Mechanical and Aerospace Engineering & Environmental Engineering and is the director of the Center for Energy and Environmental Research & Services (CEERS) in the College of Engineering at California State University, Long Beach (CSULB). He has taught various classes at the undergraduate and graduate levels in thermal sciences, supervised over 75 MS theses and projects and PhD dissertations, and published more than 100 technical papers. He has been granted patents for the development of a high-efficiency vertical axis wind turbine (VAWT) and wind turbine apparatuses and for reducing NO_X emission of Cargo Handling Equipment using a Humid Air System. He also has pending patents on a new guide-vane enclosure for capturing wind energy from passing vehicles, optimized end-plates and airfoils for improving the performance of vertical axis wind turbines, and optimized surfaces for reducing ambient NO_X. Dr. Rahai is the recipient of the 2004 Northrop Grumman Excellence in Teaching Award and the 2012 CSULB Impact Accomplishment of the Year in RSCA Award. He received the Outstanding Engineering Educator Award from the Orange County Engineering Council in California in 2014, and in 2019 he was inducted as a senior member of the National Academy of Inventors (NAI).

Rylan Moffit

Mr. Ryan Moffit is a graduate student in the joint PhD program between the CSULB College of Engineering and the Claremont Graduate University (CGU) and a Research Assistant at the Center for Energy and Environmental Research & Services (CEERS) in the College of Engineering at CSULB. Mr. Moffit is an experimentalist. His research is focused on finding an optimized surface geometry for reducing the drag of vehicles. He has authored and co-authored two ASME conference papers.

Komal Gada

Mr. Komal Gada is a graduate student in the joint PhD program between the CSULB's College of Engineering and the CGU and a Research Assistant at the CEERS in the College of Engineering at CSULB. Mr. Gada specializes in numerical optimization and computational analyses. His research is focused on the effects of coil inserts on a pipe-jet in crossflow, vehicle drag reduction, and particle transport within confined spaces. He has authored ten journal and conference papers.

Jeremy Bonifacio, PhD

Dr. Jeremy Bonifacio is a teaching professor and a senior researcher at the CEERS in the College of Engineering at CSULB. His expertise is experimental and computational fluid mechanics. He has been involved in various applied industrial projects at CEERS and is co-owner of several patents related to emission control technologies and the application of CFD in diagnosing lung diseases. Dr. Bonifacio is the winner of the CSULB 2014 innovation challenge.

MTI FOUNDER

Hon. Norman Y. Mineta

MTI BOARD OF TRUSTEES

Directors

MTI MINETA TRANSPORTATION INSTITUTE